Infrared Transmission of Contaminated Cryocooled Optical Windows

J. G. Pipes,* J. A. Roux,* A. M. Smith†
ARO, Inc., Arnold Air Force Station, Tenn.
and
H. E. Scott‡
Arnold Engineering Development Center, Arnold Air Force Station, Tenn.

Normal incidence transmission of germanium at 20, 80, 200, and 300 K is reported for wave numbers between 500 and 6700 cm^{-1} (about 1.5 to 20 μm). The absolute transmission in the 1000 to 4000 cm^{-1} region, in the absorption edge region near 6700 cm^{-1}, and in the lattice band region (500 to 800 cm^{-1}) was found to be temperature sensitive. At the cryogenic temperatures 20 and 80 K, the germanium window was employed as a substrate for the transmission study of thin solid films of NH_3, CO_2, CO, CH_4, and HCl. The spectral interval covered in the thin film study was 630 to 3700 cm^{-1}. Degradation in the transmission of a cryocooled window contaminated by these condensed gases was measured and the complex refractive index extracted from the transmission versus film thickness data for 80 K solid NH_3.

Introduction

IN order to achieve maximum detectability at long infrared (IR) wavelengths, an IR radiometer inherently employs cryogenically cooled optical components to minimize the thermal background photons. Cryogenically cooling all optical components such as filters, windows, mirrors, etc., within the field of view of the high D-star detector presents major design and operation problems. Appended to mechanical alignment problems are basic optical characteristic changes associated with cryocooling, the principal ones being degradation of reflection or transmission of optical surfaces by cryopumped gases and changes in bulk complex refractive index with temperature. Experimental programs have been conducted to obtain baseline data on mirror reflectance degradation by cryopumped gases[1]; however, data on transmission components are rather sparce. Since most transmitting components are dielectrics or semiconductors, the temperature sensitivity of their bulk complex refractive index can alter the optical characteristics of a sensor. Thus, not only is cryocontamination a problem when cooling transmission optics, but fundamental changes in absolute transmission, in absorption edge wavelength location, and in bandpass location for interference filters can be expected with cryocooling.

This paper reports the changes in absolute transmission characteristics of intrinsic germanium with cooling to 20 K and also the transmission of 80 to 20 K germanium with thin solid films of NH_3, CO_2, CO, CH_4, and HCl. The infrared spectral region studied for uncoated germanium was 500 to 6700 cm^{-1} wave numbers (about 1.5 to 20 μm wavelengths) and 630 to 3700 cm^{-1} wave numbers for the thin films. Germanium was chosen as a substrate since it has the combination of an absorption edge at 6700 cm^{-1}, a flat transmission of 47% between 1000 and 4000 cm^{-1}, and lattice absorption bands between 500 and 800 cm^{-1}. Furthermore, it is one of the most commonly employed substrates for cryocooled optical components because of its higher thermal conductivity compared to other infrared materials (except silicon). High thermal conductivity is desirable since all transmission components must be passively cooled. Complete experimental details have been given elsewhere[2]; thus, only a basic outline of the apparatus is presented here. The absolute transmission of 300, 200, 80, and 20 K germanium is first discussed followed by transmission data of 80 and 20 K germanium with thin solid films of NH_3, CO_2, CO, CH_4, and HCl ranging in thickness up to 5 μm. Finally, a theoretical model of window plus film transmission is derived and is subsequently employed with the experimental results to determine the complex refractive index of the thin film; NH_3 was used as an example. The subtractive Kramers-Kronig treatment for calculation of the film real refractive index has also been employed, and results are compared to those of the film-window model.

Received Nov. 14, 1977; presented as Paper 78-89 at the AIAA 16th Aerospace Sciences Meeting, Huntsville, Ala., Jan. 16-18, 1978; revision received May 18, 1978.

Index categories: Radiation and Radiative Heat Transfer; Thermal Surface Properties; Thermophysical Properties of Matter.

*Research Engineer, von Karman Gas Dynamics Facility.
†Research Supervisor, von Karman Gas Dynamics Facility. Associate Fellow AIAA.
‡Physicist. Member AIAA.

Instrumentation

A plan view schematic of the experimental apparatus, showing the IR interferometer (Digilab Model FTS-14), the high vacuum chamber containing the cryocooled window, and the IR source location is given in Fig. 1. The chamber is an all stainless steel cell equipped with a liquid-nitrogen (LN_2)-

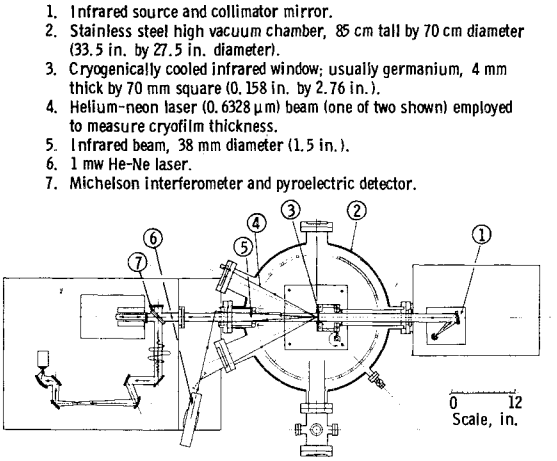

Fig. 1 Plan view schematic of the infrared optical transmission chamber (IROTC) with FTS-14 interferometer-spectrometer.

1. Infrared beam, 38-mm diameter (1.5 in.).
2. Optical stop required to underfill cryocooled window with infrared beam. Also this stop is supported by a 3-in. -ID pipe that prevents gas added to chamber from cryopumping on rear of window.
3. Aluminum holder with cryogenic passageways.
4. Infrared window heat sunk with an indium gasket to the aluminum holder.
5. Cover plate.
6. Gaseous helium or liquid nitrogen inlet and outlet.
7. Crosshatched area illustrates area of window heat sunk to holder. Clear diameter is 50.7 mm (2 in.) while infrared beam diameter is 38 mm (1.5 in.).

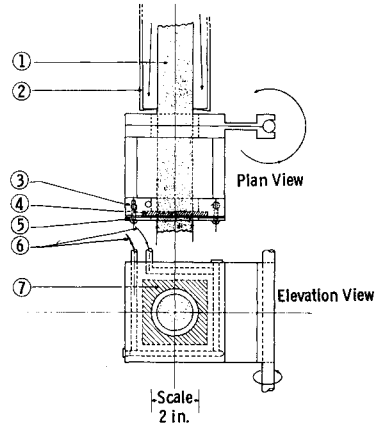

Fig. 2 Plan and elevation view of cryogenically cooled window holder.

cooled liner. A water vapor free vacuum of 10^{-8} Torr can be routinely obtained. The aluminum germanium window holder can be actively cooled with either LN_2 (80 K) or gaseous He (20 K), and, if no cryogen is employed, the holder will equilibrate with the LN_2 liner at 200 K in 12 h. Three platinum thermistors located on the window holder (see Fig. 2) gave temperature readouts accurate to 0.5 K. Important specifications on the germanium window (purchased commercially) were 1) material: intrinsic germanium of specific resistivity greater than 40 ohm-cm, 2) surface figure: ¼ wave in the visible, 3) surface quality: 40–20 scratch-dig, 4) wedge: less than 5 arc min, 5) coating: none.

Care was taken to assure that the germanium window holder did not act as an optical stop in any manner by locating a stop in the "back-of-window" gas baffle. This stop was 1.50 in. in diameter, and the clear aperture of the germanium was 2.0 in. in diameter. The radiometric absolute accuracy of the transmission arrangement was evaluated by measuring the transmission T of 300 K germanium, which should transmit near 47% at 2000 cm^{-1} since the refractive index n_g of germanium at that wave number is 4.015 and, hence,

$$T = 2n_g/(n_g^2 + 1) = 0.4690 \tag{1}$$

A typical room-temperature transmission measurement of germanium is shown in Fig. 3. Data recorded using a Perkin-Elmer prism IR spectrometer, with 1% spectral resolution, are also shown in the figure. In addition, the prism spectrometer was employed to obtain data for wavelengths from 2.5 μm to the absorption edge near 1.5 μm (not shown in Fig. 3). The two different spectrometer systems gave transmission values for the germanium window in the wave number region between 1500 and 3000 cm^{-1} that agreed to within 0.5% with calculated transmission values based on accurate real refractive index values. This agreement was used as the basis for absolute transmission accuracy of the apparatus. Outside the foregoing wave number region the signal-to-noise ratio was employed as an accuracy limit, e.g., ±1% at 3000 and 1000 cm^{-1}; ±2% at 3400 cm^{-1}; ±3% at 3700 and below 600 cm^{-1}.

The spectral resolution of the interferometer system could be selected between 16 and 0.5 cm^{-1}, but 2 cm^{-1} resolution was found to be sufficient for all work reported herein. The wave number accuracy of the interferometer is near 0.02

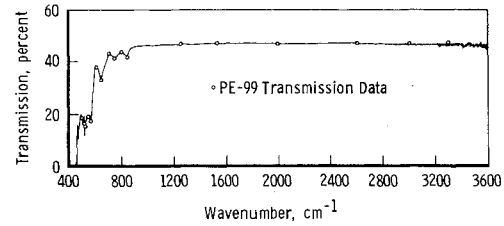

Fig. 3 Transmission of 300 K germanium window; the prism spectrometer data are compared with the interferometer data.

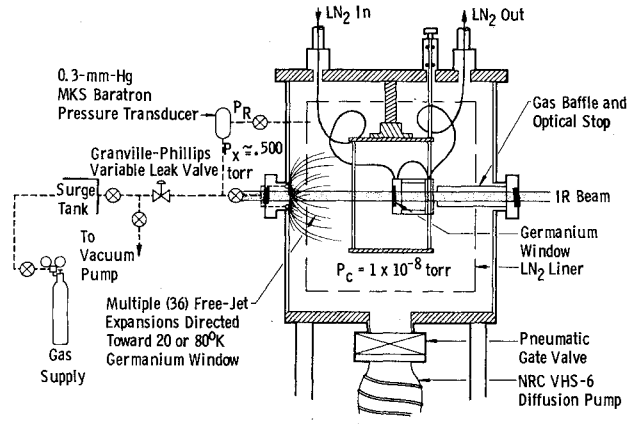

Fig. 4 Gas induction system.

cm^{-1}. Transmission measurements were performed by rotating the germanium out of the beam and recording and storing a reference power spectrum. Next, the window was rotated into the beam and the process repeated. The reference file was then divided into the sample file and plotted on a linear ordinate scale of 0-100% transmission.

Controlled contamination of the cryocooled germanium window was accomplished with the gas induction system shown schematically in Fig. 4. A toroidal-shaped header with thirty-six 1/32-in.-diam orifices spaced 10-deg apart directed the gas toward the germanium window. Gas was prevented from condensing on the back of the germanium window by a gas baffle positioned close to the back of the window holder. The gas induction system, although quite simple, worked well in that the deposition rate could be easily controlled and the final thin-film thickness was very uniform across the 2-in.-diam exposed window area. The film uniformity was judged by observing the film in the visible when the thickness corresponded to first-order interference. Color uniformity across the window indicated a thickness uniformity of 0.05 μm or better. Film uniformity and absolute thickness are two important parameters, since one objective of the experiment was to determine the complex refractive index of the thin film, a quantity derived by comparison of experimental transmission vs thickness data with a theoretical model. Any error in absolute film thickness is directly introduced into the film complex refractive index results. A dual-angle laser beam technique[3] was employed to measure the film thickness and also the film refractive index at 0.6328 μm. Basically, two He-Ne laser beams are specularly reflected off the germanium window for two different incidence angles, each measured to an accuracy of 15 arc min. As the gas is condensed, two interference patterns of different periods are monitored in the reflected laser light. If the ratio of pattern periods is termed β then the refractive index of the film is given by

$$n = [\sin^2\theta_2 - \beta^2\sin^2\theta_1]^{1/2}/[1-\beta^2]^{1/2} \tag{2}$$

where θ_1 and θ_2 are the two laser beam incidence angles. Once n has been established, the thickness d_1 of the film is readily calculated from $m\lambda = 2nd_1$, where m is the order of the in-

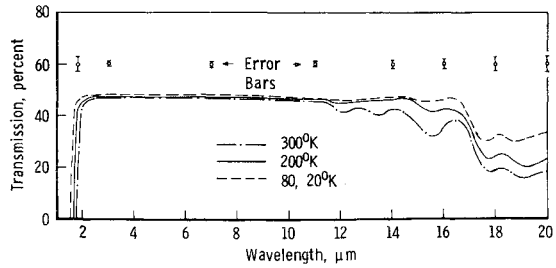

Fig. 5 Transmission of 4-mm-thick germanium window as a function of temperature; these data were recorded with prism spectrometer.

terference maxima for incidence angle $\theta_I \approx 0$ deg. The dual laser beam thickness monitor yielded thin-film refractive index values accurate to within 2%, e.g., $n = 1.42 \pm 0.02$ for 80 K NH_3 and in good agreement with the results of Seiber et al.[4] and Viehman.[5] The percent error in film thickness is numerically equal to that of the refractive index n, since $\delta\lambda/\lambda = 0$ for $\lambda = 0.6328$ μm.

Results

The transmission of the clean germanium was first measured as a function of temperature. For this measurement the prism spectrometer was employed, since data for the near IR could be obtained, i.e., the absorption edge near 1.5 μm. The measured transmission of 300, 200, 80, and 20 K germanium is shown in Fig. 5. There was an insignificant difference in the 20 and 80 K transmission but a substantial difference in the 300, 200, and 80 K data. Three basic changes in transmission signature are noted with temperature: 1) the absorption edge shifts to shorter wavelengths, about 0.2 μm for the 220 K temperature decrease, 2) the absolute transmission increases slightly in the 2- to 10-μm range and considerably in the 10- to 20-μm range because of the reduction of lattice vibration strength with cryocooling, and 3) the band centers of the far IR lattice bands shift toward shorter wavelengths, an expected result.[6]

With the transmission of the clean uncoated germanium established, the thin films condensed on the window were studied in transmission. For these measurements the interferometer was employed. Table 1 summarizes the gases and

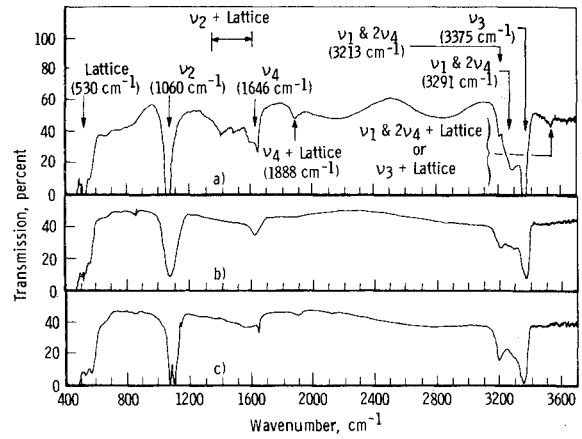

Fig. 6 Infrared transmission spectra of solid NH_3 on a germanium substrate: a) metastable I phase, deposition temperature 80 K, thickness 5.01 μm, b) amorphous phase, deposition temperature 20 K, thickness 2.12 μm, c) metastable II phase, temperature cycled 20 to 100 to 20 K, estimated thickness 2.0 μm.

important operating parameters, e.g., substrate temperature, film refractive index at 0.6328 μm, linear growth rate, etc., used in this study. Other references for the film refractive index at 0.6328 μm are also included in Table 1 for comparison. The thin-film spectra were recorded by depositing a specific gas until the first order of interference for the near normal incidence laser beam was obtained, at which time the flow was valved off and the film-window transmission measured. This procedure was repeated at each successive interference maximum until spectra for at least 10 film thicknesses had been recorded.

80 and 20 K NH_3

Transmission spectra for 23 successively thicker 80 K solid NH_3 films and for the 20 K films were recorded. Also, several 20 K films were temperature cycled to 100 K during some experiments. The spectra of the films for each condition are shown in Fig. 6. The absolute thickness of the solid NH_3 film is given in the figure caption. Assignments of the fundamental, overtone, and combination frequencies of cubic crystalline NH_3 has been reported by Reding and Hornig.[7]

Table 1 Growth conditions for solid gases studied

Solid gas	Substrate temp., K	Refractive index at He-Ne 0.6328 μm	Linear growth rate, μm/min	Inlet pressure (MKS Baratron), μm Hg	Background pressure during deposition, Torr	Equilibrium vapor pressure, Torr, at substrate temp.	Grade of gas employed
NH_3 [a]	80	1.42 ± 0.02	1.60	600	3×10^{-7}	6×10^{-11}	Ultrahigh pure, 99.999%
NH_3 [a]	20	1.42 ± 0.02	2.80	600	4×10^{-7}	$< 10^{-13}$	Ultrahigh pure, 99.999%
NH_3 [b]	30-60	1.38 ± 0.02					
CO_2 [a]	80	1.42 ± 0.02	1.85	500	1×10^{-6}	8×10^{-8}	Coleman grade, 99.999%
CO_2 [a]	20	1.42 ± 0.02	1.85	500	1×10^{-6}	$< 10^{-13}$	Coleman grade, 99.999%
CO_2 [b]	24,77	1.34 ± 0.06					
CO_2 [c]	82	1.42 ± 0.06	1.3				High purity, 99.98%
CO_2 [d]	77	1.41					
CO	20	1.22 ± 0.02	1.04	500	4×10^{-6}	5×10^{-13}	Ultrahigh pure, 99.8%
CH_4	20	1.38 ± 0.02	4.13	150	5×10^{-7}	$< 10^{-13}$	Instrument grade, 99.7%
HCl	20		1.30	500	3×10^{-7}	$< 10^{-13}$	Electronic grade, 99.99%

[a] From this study. [b] From Ref. 1. [c] From Ref. 4. [d] From Ref. 5.

More recently Wolff et al.[8] reinvestigated the infrared spectra of crystalline NH_3, NH_2D, ND_2H, and NH_3 (deposition temperature of 113 K) and concluded that the ν_1 and $2\nu_4$ could not be assigned to the 3291 and 3213 cm^{-1} frequencies, but that both vibrations contribute to the observed frequencies. Staats and Morgan[9] have discussed the possible crystalline phase of solid NH_3 deposited at different substrate temperatures and deposition rates. Staats and Morgan reexamined the infrared spectrum of solid NH_3 after the X-ray diffraction study of solid NH_3 reported by Mauer and McMurdie[10] gave evidence of two metastable low-temperature phases. Staats and Morgan found that solid NH_3 can exhibit two metastable phases as well as the cubic structured phase; their deposition temperatures were 77 K for metastable II, 112 K for metastable I, and 150 K (or 77 K warmed to 150 K) for cubic NH_3. The phase or crystalline structure is quite important with regard to optical transmission degradation: a clear nonscattering crystalline cryofilm would only degrade transmission of an optical component near the fundamental, combination, and overtone bands, whereas a metastable or an amorphous cryofilm could with changes in temperature transform to a highly scattering cryofilm.

In this study three different phases of solid NH_3 were observed and will be classified based on the X-ray data of Mauer and McMurdie and the infrared spectra of Staats and Morgan. The 80 K NH_3 is believed to be a metastable I phase, the 20 K NH_3 an amorphous phase, and the 20 K NH_3 warmed to 100 K and recooled to 20 K a metastable II phase (see Fig. 6). A cubic phase, obtained by deposition above 140 K (a conclusion from the X-ray data) could not be observed, since this temperature is above the LN_2 chamber liner temperature and all the gas admitted into the chamber would condense on the liner, not an optical component, at 140 K. The 20 K spectrum of Fig. 6b is undoubtedly that of an amorphous film since the lattice band (ν_5) at 530 cm^{-1} is not present. Also, the fundamental bands are broad, 100 cm^{-1} full width half maximum (FWHM) for the ν_2 band, compared to the 80 K NH_3 ν_2 band, 25 cm^{-1} FWHM, a characteristic of an amorphous solid. The assignment of the metastable II phase to the temperature cycled NH_3 film is consistent with that of Staats and Morgan. No crystalline structure has been assigned to this phase and it is possible that this film was a mixture of phases. Also, an assignment of a vibrational mode for the feature at 1090 cm^{-1} has not been made (see Fig. 6c). The 1060 cm^{-1} is the ν_2 symmetric deformation, as was evident in the 80 K deposit, and the 1090 cm^{-1} may well be this same deformation but for a different crystalline structure. Staats and Morgan also observed this behavior for 77 K deposits grown from a 160 K NH_3 source. This growth condition is similar to the history of our temperature cycled 20 K deposit since gas released during warmup is recondensed to some extent after recooling to 20 K but is of a much lower (unknown) ambient temperature than the original source temperature. The indication is that the source temperature may govern the deposit phase to a significant extent.

In all cases the 20 K NH_3 films were cloudy or milky in visible light compared to the very clear 80 K films. This is the primary reason why only ten 20 K film thicknesses were obtainable since the He-Ne laser interference pattern dropped in amplitude because of scattering by the film as the film thickness reached the order of 2 μm. The effect on infrared transmission of the 20 K scattering film is evident in Fig. 6b since the peak transmission should be close to 60% in nonabsorbing regions, as was the case for the thinner deposits; however, only values up to 50% transmission are seen. This is a 10% loss in transmission attributable to scattering for infrared wavelengths in a 2-μm thick film, whereas in visible light the polished geranium window could not be distinguished because of much greater scattering. The degradation in transmission of a cryofilm contaminated window is thus due to scattering and molecular band absorption. The presence of an infrared inactive film would only cause an increase or no change in transmission since it acts as an antireflection coating. This effect is clear in Fig. 6a near 2500 cm^{-1}.

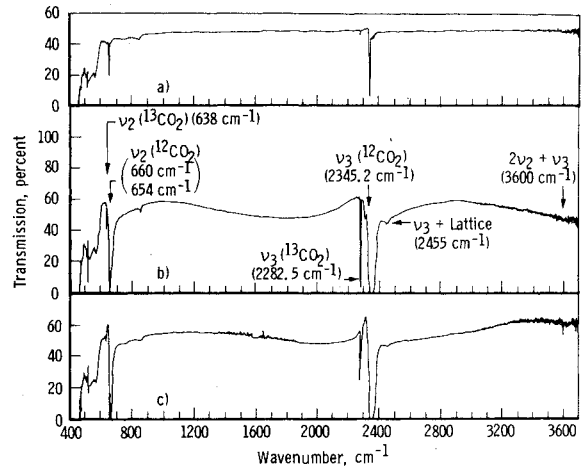

Fig. 7 Infrared transmission spectra of solid CO_2 on a germanium substrate: a) deposition temperature 80 K, thickness 0.11 μm (the window transmission is degraded only near the fundamental frequencies); b) deposition temperature 80 K, thickness 1.67 μm, c) deposition temperature 20 K, thickness 1.89 μm (the line shapes indicate the 20 K CO_2 is also cubic structured).

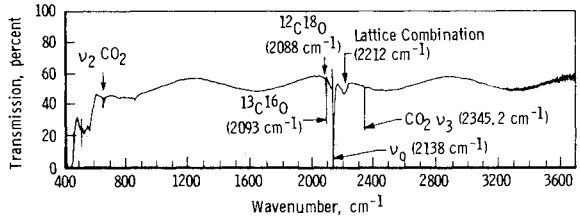

Fig. 8 Infrared transmission spectrum of 5.057-μm-solid CO on a 20 K germanium substrate.

80 and 20 K CO_2

All solid 80 and 20 K CO_2 films had a cloudy appearance in visible light. The infrared spectra of 80 and 20 K CO_2 films are shown in Fig. 7. The absorption bands for solid CO_2 are given in Fig. 7b and are responsible for the major transmission degradation in the thinner films. The channel spectrum alters the window transmission to a significant extent only as the film becomes thicker, i.e., greater than 0.5 μm. Since the refractive index for 20 K CO_2 at 0.6328 μm could not be accurately measured with the dual laser beam technique because of severe scattering, the value employed was 1.42, the same as 80 K CO_2. Although the infrared spectra of 20 K and 80 K CO_2 are quite similar, indicating similar IR refractive indices, there could be errors in the absolute thickness of the 20 K CO_2 films of up to 12%. Both the 20 and 80 K CO_2 films were temperature cycled, 20 K up to 50 K and 80 K up to 100 K, and no phase transition was detected based on the infrared signature. It is thus believed that the cubic structure persists for all deposition temperatures above 20 K.

20 K CO

Carbon monoxide had to be deposited at the lower temperatures because of its high equilibrium vapor pressure at 80 K. The CO films were nonscattering, and thus a total of 25 different film thicknesses were deposited and infrared spectra recorded. The refractive index of 20 K CO at 0.6328 μm was found to be 1.22 $\pm$0.02. A typical transmission spectrum of a solid CO film (5.057-μm thick) is shown in Fig. 8, from which it is clear that the fundamental stretching mode ν_0 at 2138 cm^{-1} is the main absorption feature; the bands at 2345.2 and

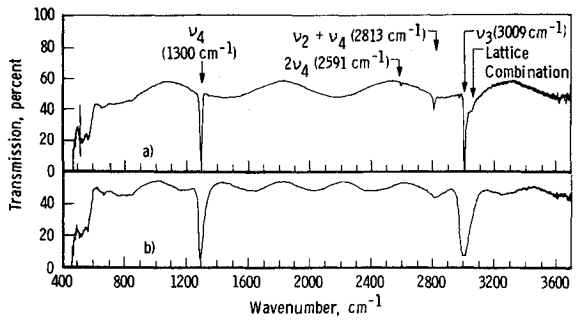

Fig. 9 Infrared transmission spectra of solid CH_4 on a germanium substrate: a) deposition temperature 20 K, thickness 5.04 μm, b) temperature cycled 20 to 50 to 20 K, estimated thickness 9 μm.

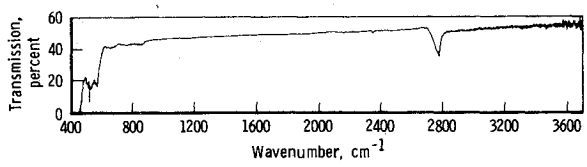

Fig. 10 Transmission of 0.3-μm-solid HC1 on a 20 K germanium window.

660 cm^{-1} are a result of CO_2 impurity in the CO source. The weak features at 2088 and 2093 cm^{-1} are due to $^{12}C^{18}O$ and $^{13}C^{16}O$ isotopes, respectively. The broad absorption at 2212 cm^{-1} is a fundamental plus lattice mode similar to the ν_3 + lattice band in the solid CO_2 films at 2455 cm^{-1}. On one occasion a rather thick (~15 μm) CO film was warmed to 50 K then recooled to 20 K. No change in the band structure was observed; thus CO apparently does not undergo a phase transformation in this temperature range.

20 K CH_4

Methane can only be studied at the lower temperatures because of its high vapor pressure at 80 K. The transmission of a 5-μm solid film of 20 K CH_4 is shown in Fig. 9a. The measured refractive index at 0.6328 μm is 1.38 ±0.02, which compares favorably with the value of 1.30 ±0.01 (91 K, $\lambda = 0.583$ μm) from Ref. 11. The two fundamental absorption bands are indicated in Fig. 9a. Further, the $2\nu_4$ (2591 cm^{-1}) and the $\nu_2 + \nu_4$ (2813 cm^{-1}) are seen in the thicker deposits, and again a lattice combination band is evident near 3050 cm^{-1}. As the methane was temperature cycled (20 to 50 K) an interesting phase transformation took place. Figure 9b shows the infrared spectrum of this temperature cycled CH_4 (the thickness is uncertain but is estimated to be 9 μm) and it is clear that the ν_3 and ν_4 bands have become much broader, 90 cm^{-1} FWHM for ν_3 compared to 20 cm^{-1} FWHM for the 20 K CH_4, and also not as intense. The $\nu_2 + \nu_4$ band has also become much broader. As the deposit transformed to an as yet undetermined phase, it became highly scattering as seen in visible light, and also the near infrared transmission dropped 5% because of scattering. The broad and weak nature of the ν_3 and ν_4 bands in the new phase CH_4 are indicative of an amorphous solid. Thus, it is believed that this phase is a metastable phase that the CH_4 solid passes through as it transforms to an alternate crystalline phase from the 20 K crystalline phase as the temperature is raised.

20 K HC1

The HC1 deposits were generally of the scattering type and only a few thicknesses were deposited. Since the 0.6328-μm refractive index could not be measured, the thickness of the HC1 film of Fig. 10 is unknown (deposition was stopped at the second He-Ne interference minimum, thus the film is probably near 0.3-μm thick).

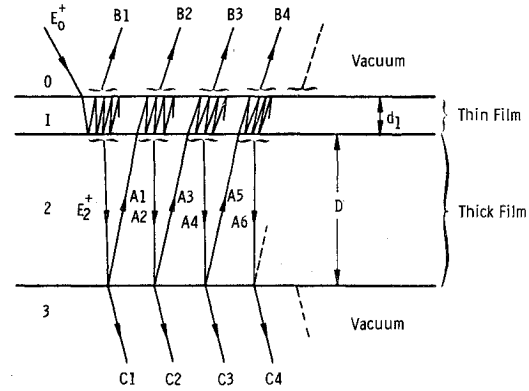

Fig. 11 Geometry depicting analytical model for a thin film formed upon a thick film.

Optical Constants of Solid Ammonia

In order to extract the complex refractive index ($\tilde{n} = n - ik$) of the thin solid film on a thick germanium window from the transmission vs thickness data, an analytical model of film plus window transmission was derived. Unlike the thin film, it is assumed that the germanium window is a thick film and there is no phase coherence between multiple internal reflected rays within the window. Moreover, the real part of the germanium complex index n_g is known and given in Ref. 12 as

$$n_g = A + BL + CL^2 + D\lambda^2 + E\lambda^4 \tag{3}$$

where λ is in μm and $L = (\lambda^2 - 0.028)^{-1}$, $A = 3.99931$, $B = 0.391707$, $C = 0.163492$, $D = -0.000006$, $E = 0.00000053$. This analytical form matches the observed values given in Ref. 13 to ±0.07% for 300 K germanium. We have adjusted the constant A so that the calculated transmission for 80 K germanium agreed with the observed values. The geometry describing the transmission is shown in Fig. 11. For convenience the different layers have been subscripted 0, 1, 2, and 3. The model employed to fit the experimental results is for normal incidence only. The rigorous derivation of the total external transmission for the model shown in Fig. 11 is given in Ref. 2; the final result being

$$T = \frac{T_2 T_{012} e^{-\alpha_g D}}{1 - R_2 R_{210} e^{-2\alpha_g D}} \tag{4}$$

for an absorbing thin film on an absorbing thick window, where D = the thickness of the substrate, $\alpha_g = 4\pi k_g/\lambda$ is the absorption coefficient of the substrate, k_g = imaginary component of the complex refractive index of the substrate, and λ is the wavelength in vacuum. T_2 designates the power transmission from medium 2 to medium 3, T_{012} designates the power transmission from medium 0 to medium 2 after undergoing thin film interference in medium 1, R_2 designates power reflected at medium 3 incident from medium 2, and R_{210} designates the power reflection coefficient of radiation which is incident from medium 2 and is reflected back into medium 2 after undergoing thin-film interference in medium 1. T_2, T_{012}, R_2, and R_{210} are algebraically complicated expressions but are explicitly calculable and are given in Ref. 14 in terms of the wavelength and the thin film's thickness along with its optical properties as well as those of the substrate.

The 80 K NH_3 data, 16 different film thicknesses in all, were chosen to be used in a least-squares determination of the optical constants of 80 K solid NH_3. The transmission data were digitized every 10 cm^{-1}. A typical example of the agreement of the experimental data with the analytical model is given in Fig. 12 for several wavelengths. The final $\tilde{n} = n - ik$ found by the least-squares fit is employed in Eq. (4) to compute the transmission vs thickness curve. Similar excellent

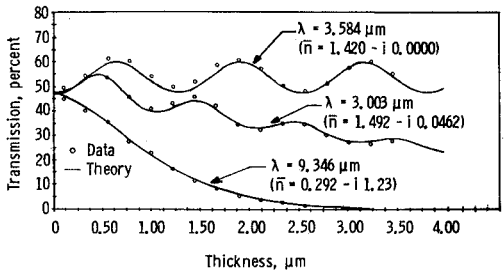

Fig. 12 Comparison of theory and data for 80 K solid NH_3 for three different wavelengths; complex refractive indices of 80 K solid NH_3 employed in the analytical model are given in the figure.

agreement was the case for all wave numbers between 700 and 3700 cm^{-1} even in the regions of absorption fundamentals. α_g in Eq. (4) was taken to be zero (nonabsorbing substrate) for all computations of $\bar{n}$ and T for 80 K solid NH_3. The values of $\bar{n}$ for all wave numbers are plotted in Fig. 13 and listed in Table 2. These results are in good agreement with the recently published values of 188 K NH_3 by Robertson et al.[15] with the exception that the maximum and minimum values of n in the absorption bands are higher and lower, respectively, indicating a better spectral resolution in our data and also possibly a breakdown in accuracy of the Kramers-Kronig techniques, employed by Robertson et al., near the absorption frequencies. In Fig. 13b the dashed line represents the minimum imaginary refractive index values that can be determined due to the error limits on the film-window transmission measurements.

Finally, because of its simplicity, the subtractive Kramers-Kronig[15] relation between n and k was used in comparison with the least-squares determination of n. The subtractive Kramers-Kronig relation is given by

$$n(\nu) = n(\nu_m) + \frac{2}{\pi} P \int_0^\infty \left[\frac{k(\nu')\nu' - k(\nu)\nu}{(\nu')^2 - \nu^2} - \frac{k(\nu')\nu' - k(\nu_m)\nu_m}{(\nu')^2 - \nu_m^2} \right] d\nu' \tag{5}$$

where ν_m is a reference frequency, 2500 cm^{-1} in this work, and P indicates the Cauchy principal value of the integral. The integral was evaluated by the simple trapezoidal rule. The $k(\nu')$ values used in Eq. (5) are those listed in Table 2. Shown in Fig. 13 is a comparison between the least-squares and subtractive Kramers-Kronig determination of n. The 80 K NH_3 data are in excellent agreement between the two techniques. The subtractive Kramers-Kronig results are only shown for comparison purposes; the least-squares determination of n and k is believed to be accurate as is borne out by the agreement between theory and data.

Summary

The infrared transmission of cryocooled germanium with and without thin films of condensed gases has been determined. Temperatures of the substrate were 80 and 20 K, and the gases condensed were NH_3, CO_2, CO, CH_4, and HCl. The effects of cryocooling germanium were established from the near-infrared absorption edge to the 20-μm lattice bands. For all of the condensed gases studied the infrared spectrum was measured as a function of thickness; the effect of temperature cycling was established; the phase transitions, if they existed, were noted; and the scattering nature of the condensed gases was qualitatively discussed. For 80 K solid NH_3 the complex refractive index was determined by a least-squares fit of a derived analytical model to the experimental

Table 2 Complex refractive index ($\bar{n} = n - ik$) of 80 K solid NH_3

ν, cm^{-1}	$n(\nu)$	$k(\nu)$	ν, cm^{-1}	$n(\nu)$	$k(\nu)$	ν, cm^{-1}	$n(\nu)$	$k(\nu)$	ν, cm^{-1}	$n(\nu)$	$k(\nu)$
700	1.352	2.02×10^{-2}	1200	1.318	1.44×10^{-2}	1800	1.381	7.18×10^{-4}	3000	1.432	$<1.0\times10^{-6}$
720	1.363	1.62	1220	1.330	1.33	1820	1.385	1.56×10^{-3}	3050	1.435	
740	1.384	1.42	1240	1.341	9.75×10^{-3}	1840	1.387	2.70	3100	1.439	
760	1.383	1.56	1260	1.349	6.75	1860	1.389	5.77	3150	1.445	
780	1.404	1.62	1280	1.362	5.91	1880	1.388	1.18×10^{-2}	3160	1.446	1.77×10^{-5}
800	1.414	1.56	1300	1.366	8.88	1900	1.383	1.11	3180	1.453	2.34×10^{-3}
820	1.428	1.30	1320	1.372	1.04×10^{-2}	1920	1.383	7.60×10^{-3}	3190	1.454	4.87
840	1.421	1.69	1340	1.378	9.86×10^{-3}	1940	1.383	4.27	3200	1.458	1.08×10^{-2}
860	1.414	1.85	1360	1.382	1.39×10^{-2}	1960	1.384	2.14	3220	1.457	1.58
880	1.468	9.48×10^{-3}	1380	1.389	1.90	1980	1.388	1.37	3240	1.470	2.16
900	1.494	7.60	1400	1.392	2.85	2000	1.387	6.93×10^{-4}	3260	1.463	3.60
920	1.511	6.75	1420	1.383	2.60	2020	1.388	3.19	3280	1.475	5.61
940	1.537	6.32	1440	1.378	2.22	2040	1.391	$<1.0\times10^{-6}$	3300	1.465	5.55
960	1.573	7.81	1460	1.385	1.48	2050	1.391		3320	1.472	4.62
980	1.602	1.18×10^{-2}	1480	1.388	1.78	2100	1.394		3340	1.504	4.62
1000	1.650	2.60	1500	1.390	2.28	2150	1.397		3360	1.676	15.8
1010	1.699	2.85	1520	1.392	1.95	2200	1.398		3370	0.981	57.1
1020	1.776	4.16	1540	1.393	1.78	2250	1.400		3380	0.217	57.1
1030	1.899	5.48	1560	1.394	1.85	2300	1.401		3390	1.103	3.23
1040	2.119	11.7	1580	1.395	3.25	2350	1.405		3400	1.229	7.78×10^{-3}
1050	2.400	55.5	1600	1.395	4.44	2400	1.405		3410	1.275	3.70
1060	1.041	269.0	1620	1.387	4.49	2450	1.409		3420	1.299	2.22
1070	0.292	123.0	1640	1.375	5.07	2500	1.413		3440	1.328	2.02
1080	0.513	30.2	1650	1.375	6.08	2550	1.415		3460	1.341	1.71
1090	0.947	11.8	1660	1.344	1.89	2600	1.417		3480	1.348	2.22
1100	1.001	7.21	1670	1.353	3.43×10^{-3}	2650	1.418		3500	1.354	1.67
1110	1.048	4.88	1680	1.356	5.96×10^{-4}	2700	1.417		3520	1.360	2.37
1120	1.120	3.34	1690	1.363	1.00	2750	1.419		3540	1.356	2.02
1130	1.175	2.31	1700	1.368	1.72	2800	1.421		3560	1.373	$<1.0\times10^{-6}$
1140	1.212	2.37	1720	1.370	3.02	2850	1.422		3600	1.385	
1150	1.239	1.77	1740	1.376	7.04	2900	1.425		3650	1.389	
1160	1.262	1.89	1760	1.376	6.15	2950	1.429		3700	1.387	
1180	1.294	1.62	1780	1.378	9.74						

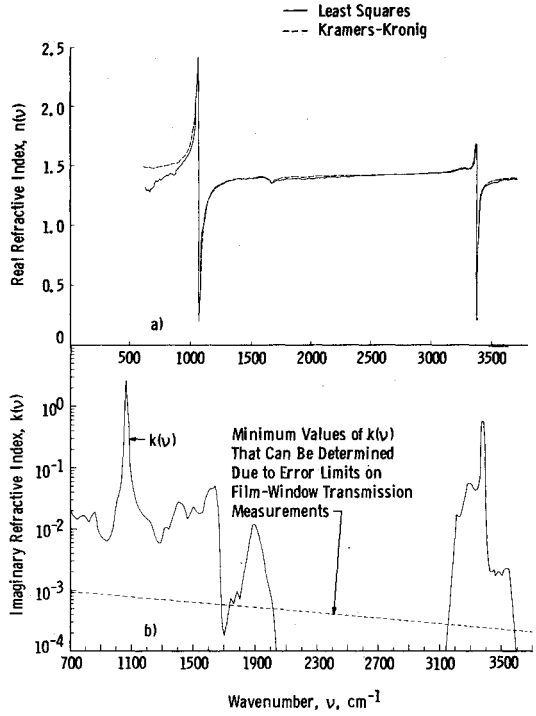

Fig. 13 Complex refractive index for 80 K solid NH_3: a) real component, b) imaginary component.

data. The $\tilde{n}$ values of 80 K NH_3 for 700 to 3700 cm^{-1} wave numbers are believed to be the most accurate values to date. The complex refractive indices of solid CO_2, CO, CH_4, H_2O, O_2, and N_2 will be reported in a later publication.

Acknowledgment

The research reported herein was performed by the Arnold Engineering Development Center (AEDC), Air Force Systems Command (AFSC). Work and analysis was done by personnel of ARO, Inc., a Sverdrup Corporation Company, operating contractor of AEDC. Further reproduction is authorized to satisfy needs of the U.S. Government.

References

[1] Thompson, S.B., Arnold, F., Sanderson, R.B., and Mantz, A.W., "Optical Properties of Cryodeposits on Low Scatter Mirrors," AIAA *Progress in Astronautics and Aeronautics: Thermophysics and Spacecraft Thermal Control,* Vol. 35, edited by R.G. Hering, New York, 1974, pp. 229–248.

[2] Pipes, J.G., Roux, J.A., Smith, A.M., and Scott, H.E., "Transmission of Infrared Materials and Condensed Gases at Cryogenic Temperatures," Arnold Engineering Development Center, Arnold Air Force Station, Tenn., AEDC-TR-77-71, Sept. 1977.

[3] Tempelmeyer, K.E. and Mills, D.W., Jr., "Refractive Index of Carbon Dioxide Cryodeposit," *Journal of Applied Physics,* Vol. 39, May 1968, pp. 2968–2969.

[4] Seiber, B.A., Smith, A.M., Wood, B.E., and Müller, P.R., "Refractive Indices and Densities of H_2O and CO_2 Films Condensed on Cryogenic Surfaces," *Applied Optics,* Vol. 10, Sept. 1971, pp. 2086–2089.

[5] Viehman, W., (personal communication), NASA Goddard Space Flight Center, Greenbelt, Md.

[6] Collins, R.J. and Fan, H.Y., "Infrared Lattice Absorption Bands in Germanium, Silicon, and Diamond," *Physical Review,* Vol. 93, Feb. 1954, pp. 674–678.

[7] Reding, F.P. and Hornig, D.F., "The Vibrational Spectra of Molecules and Complex Ions in Crystals. V. Ammonia and Deutero-Ammonia," *Journal of Chemical Physics,* Vol. 19, May 1951, pp. 594–601.

[8] Wolff, H., Rollar, H.G., and Wolff, E., "Infrared Spectra and Vapor Pressure Isotope Effect of Crystallized Ammonia and its Deuterium Derivatives," *Journal of Chemical Physics,* Vol. 55, Aug. 1971, pp. 1373–1378.

[9] Staats, P.A. and Morgan, H.W., "Infrared Spectra of Solid Ammonia," *Journal of Chemical Physics,* Vol. 31, Aug. 1959, pp. 553–554.

[10] Mauer, F.A. and McMurdie, H.F., *American Crystallographic Association Meeting,* June 1958.

[11] Marcoux, J.E., "Indices of Refraction of Some Gases in the Liquid and Solid State," *Journal of the Optical Society of America,* Vol. 59, Aug. 1969, p. 998.

[12] Herzberger, M. and Salzberg, C.D., "Refractive Indices of Infrared Optical Materials and Color Correction of Infrared Lenses," *Journal of the Optical Society of America,* Vol. 52, April 1962, pp. 420–426.

[13] Moses, A.J., "Refractive Index of Optical Materials in the Infrared Region," Hughes Aircraft Co., Culver City, California, DS-166, Jan. 1970.

[14] Heavens, O.S., *Optical Properties of Thin Solid Films,* Academic Press, New York, 1955.

[15] Robertson, C.W., Downing, H.D., Curnutte, B., and Williams, W., "Optical Constants of Solid Ammonia in the Infrared," *Journal of the Optical Society of America,* Vol. 65, April 1975, pp. 432–435.